



Development of High-Power and High-Efficiency Motor for a Newly Developed Electric Vehicle

Author(s): Shunji Oki, Shigeaki Ishikawa and Takeshi Ikemi

Source: *SAE International Journal of Alternative Powertrains*, Vol. 1, No. 1 (June 2012), pp. 104-111

Published by: SAE International

Stable URL: <https://www.jstor.org/stable/10.2307/26168969>

REFERENCES

Linked references are available on JSTOR for this article:

https://www.jstor.org/stable/10.2307/26168969?seq=1&cid=pdf-reference#references_tab_contents

You may need to log in to JSTOR to access the linked references.

JSTOR is a not-for-profit service that helps scholars, researchers, and students discover, use, and build upon a wide range of content in a trusted digital archive. We use information technology and tools to increase productivity and facilitate new forms of scholarship. For more information about JSTOR, please contact support@jstor.org.

Your use of the JSTOR archive indicates your acceptance of the Terms & Conditions of Use, available at <https://about.jstor.org/terms>



JSTOR

SAE International is collaborating with JSTOR to digitize, preserve and extend access to *SAE International Journal of Alternative Powertrains*

Development of High-Power and High-Efficiency Motor for a Newly Developed Electric Vehicle

Shunji Oki, Shigeaki Ishikawa and Takeshi Ikemi
Nissan Motor Company Ltd.

ABSTRACT

This paper describes the development of the drive motor used on a newly developed electric vehicle (EV) that has been specifically designed and engineered as the world's first mass-produced EV. Producing maximum torque of 280 Nm and maximum power of 80 kW, this synchronous motor was selected as the first electrified powertrain to be named to Ward's 10 Best Engines list for 2011. In developing this motor, magnetic field simulations were conducted in the process of adopting the following in-house technologies to achieve a compact motor size, high output and high efficiency.

The rotor shape has the interior permanent magnets arranged in a V-shaped that achieves a superior balance of torque and power. The flux barriers located on the outer periphery are designed to reduce iron loss. The V-shaped flux barriers provide both excellent mechanical strength and outstanding performance during high-speed motor operation. The motor is built with segmented magnets that reduce eddy current losses to improve continuous output performance.

The results of magnetic field simulations and mechanical strength simulations are presented along with a description of each of the unique technologies adopted.

CITATION: Oki, S., Ishikawa, S. and Ikemi, T., "Development of High-Power and High-Efficiency Motor for a Newly Developed Electric Vehicle," *SAE Int. J. Alt. Power.* 1(1):2012, doi:10.4271/2012-01-0342.

INTRODUCTION

For the automotive industry, the development of zero-emission vehicles that have virtually no environmental impact during operation represents the optimum long-term approach to protecting the environment and generating product demand. At Nissan, we have positioned the introduction and popularization of zero-emission electric vehicles (EVs) at the core of our corporate strategy and are committed to being a global leader in zero-emission vehicles.

The company has released and marketed numerous EV models since putting its first EV on the market in 1947. A mass-produced EV model for global markets and featuring dedicated styling and design has been successively released in the United States, Japan and Europe since late 2010.^[1] The 80-kW AC synchronous electric motor powering the new Nissan LEAF EV became the first drive motor in history to be named to Ward's 10 Best Engines list for 2011.

This paper describes the innovative technologies incorporated in this electric motor.

MOTOR OVERVIEW

The motor and inverter have been developed specifically for a newly developed EV, which involved optimizing the relationship between current and torque/power output. Figure 1 shows the relationship between the characteristics of the electric powertrain and the required vehicle performance in terms of driving force and vehicle speed. With the electric powertrain supplying maximum torque of 280 Nm and maximum power of 80 kW, the newly developed EV provides ample practical performance comparable to that of gasoline-engine vehicles, including a top speed of 145 km/h and gradability of 30%.

The efficiency of the electric powertrain is shown in Figure 2. In this figure, the electric powertrain comprises the motor, inverter and AC cables connecting them. The system achieves high efficiency of nearly 95% at the most efficient operating point. At the weighted average of the operating points used most frequently by the vehicle, this electric powertrain still delivers high efficiency of over 90%.

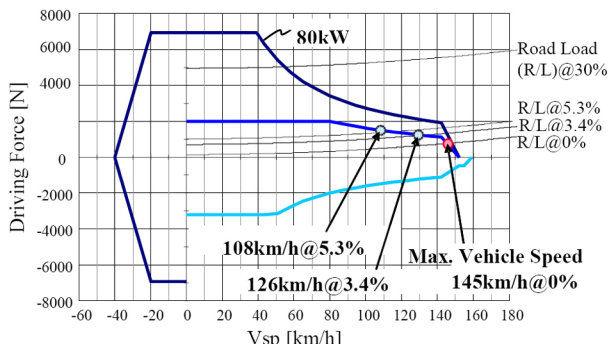


Figure 1. Dynamic performance

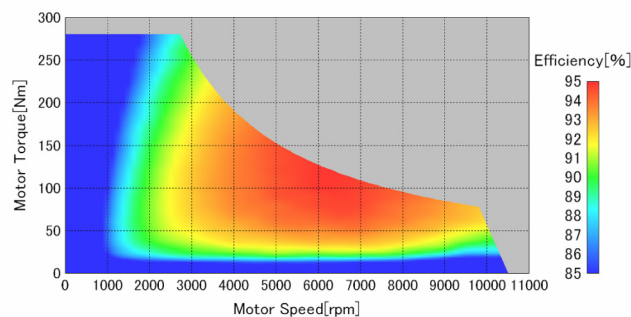


Figure 2. Efficiency of the electric powertrain

The drive motor used on the newly developed EV is an interior permanent magnet synchronous motor (IPM) with an original design adapted to the ways in which EVs are driven. Compact in size, it delivers high power and efficiency to support the quick response characteristic of EVs.

In Japan, Nissan released Prairie Joy EV in 1996 and released Hyper-mini in 2000. We learned the motor performance required for EV from the experience. The drive motor used on the newly developed EV is based on the drive motors used on our fuel cell vehicles, the 2003 model X-TRAIL FCV rolled out for limited leasing in 2003 and the subsequent 2005 model X-TRAIL FCV released for limited leasing in 2005. It was developed with performance specifications targeted specifically for EV use and is being manufactured in-house.

The external appearance of the motor is shown in Figure 3, and its specifications are listed in Table 1 in comparison with those of the drive motor used on the Hypermini. Generating maximum torque of 280 Nm and maximum power of 80 kW, the motor provides the high levels of performance required of EV drive motors and attains a top speed of 10,390 rpm.



Figure 3. Appearance of motor

Table 1. Comparison of motor specifications

Performance	Newly developed	Hypermini
Max. torque	280 Nm	130 Nm
Max. power	80 kW	24 kW
Top motor speed	10,390 rpm	6,700 rpm
Motor mass	Approx. 58 kg	Approx. 54 kg
Cooling	Water	Water

MAGNETIC CIRCUIT DESIGN

A permanent magnet synchronous motor generates torque in accordance with the expression in Eq. (1), where P is the number of poles, ϕ_a is the interlinkage magnetic flux, L_d and L_q are the inductance of the dq axes, and i_d and i_q represent the current of the dq axes.

$$T = \frac{P}{2} \left\{ \phi_a i_q + (L_d - L_q) i_d i_q \right\} \quad (1)$$

Here, the first and second terms of Eq. (1) express the permanent magnet torque and reluctance torque, respectively.

Because an interior permanent magnet (IPM) motor generally has inverse saliency, $L_d < L_q$ and $(L_d - L_q)$ is negative, making it possible to obtain positive reluctance torque by controlling i_d using a negative value. It is clear that ways of increasing torque under a given current level including making ϕ_a larger or increasing the inductance difference $(L_d - L_q)$, i.e., increasing L_q and reducing L_d .

On the other hand, let us consider the motor output in the region of field-weakening control that controls the back EMF of the motor at high speeds so that it does not exceed the battery voltage. As shown in Fig. 5, the maximum motor output increases as the ratio of the interlinkage magnetic flux ϕ_a to the d-axis inductance L_d (ϕ_a/L_d) becomes larger.

However, as (ϕ_a / L_d) increases, the field-weakening current needed to control the motor output to a zero state also increases. Consequently, efficiency declines in the low output region and also more current is needed to produce the desired output, thus requiring a larger drive inverter. Therefore, in designing the magnetic circuit of a motor, it is essential to design motor constants (ϕ_a , L_d and L_q) that match the desired torque and power levels.

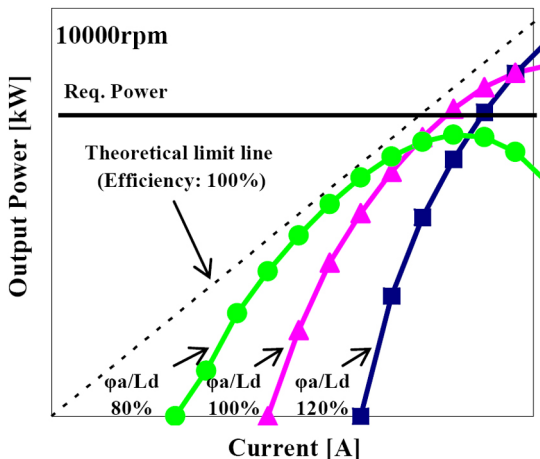


Figure 5. Motor output for various parameters

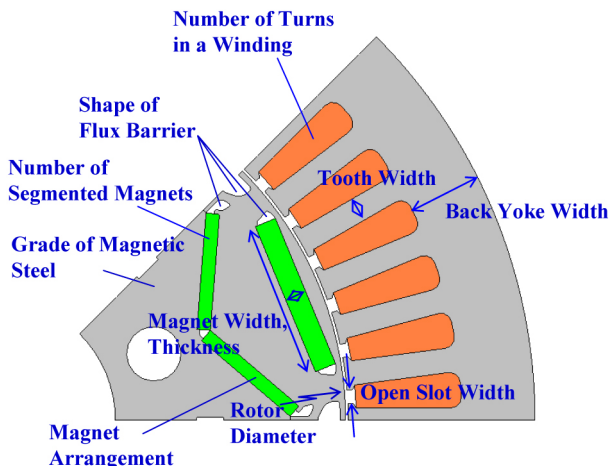


Figure 6. Parameters for magnetic circuit design

In order to achieve these motor constants, it is necessary to optimize many motor parameters as shown in Fig. 6. The electromagnetic steel sheet used in motors is characterized by magnetic saturation and nonlinear properties. Moreover, the rotor also has a complex shape. For these reasons, magnetic field simulations and strength simulations were used to examine the shape of each part. Figure 7 shows a typical example of the results of a magnetic field simulation.

The following sections describe the results obtained in this study concerning the magnet arrangement, flux barrier geometry and magnet segmentation, which are three especially important shape elements of the rotor of an EV motor. These results were incorporated in the motor used on the new EV.

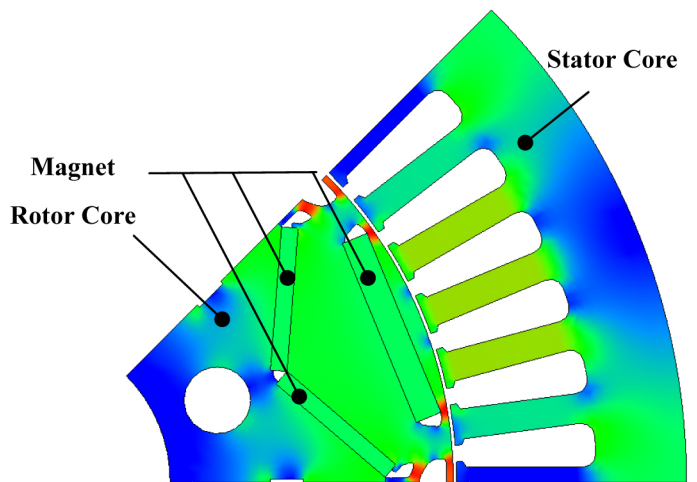


Figure 7. Magnetic field simulation results

MAGNET ARRANGEMENT

An IPM motor allows more degrees of design freedom than a surface permanent magnet (SPM) motor because the magnets can be embedded. The type of magnet arrangement that is selected is particularly important because it has a profound impact on motor characteristics. [2]

In developing the motor for the new EV, a comparative study was made of an I-shaped, a V-shaped and a ∇ -shaped magnet arrangement in order to select the best type for the motor. Figures 8,9,10 show the rotor shapes that were examined in this study.

A constant quantity of magnets was used in each case in order to compare accurately the motor characteristics attributable to the differences in the magnet arrangement. A centrifugal force analysis was conducted to determine the bridge shape at the ends of the magnets so that the stresses generated in the electromagnetic steel sheet would be equal. In addition, the layer thickness, stator geometry, number of turns, and current were the same in each case and the motor output characteristics were calculated in magnetic field simulations.

Figure 11 compares the maximum torque obtained with each magnet arrangement and Figure 12 compares their maximum power in the high-speed region.

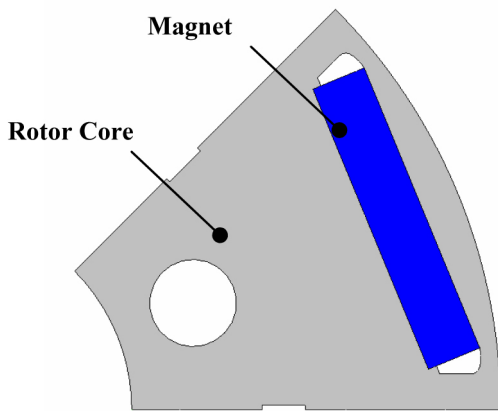


Figure 8. I-shaped rotor geometry

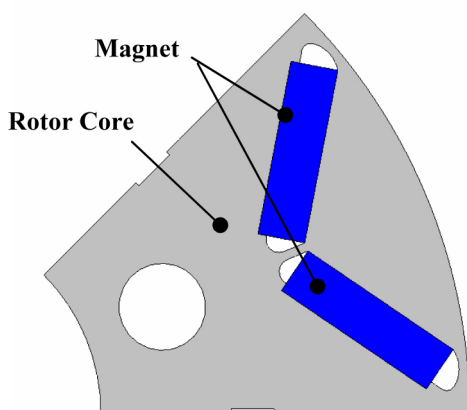


Figure 9. V-shaped rotor geometry

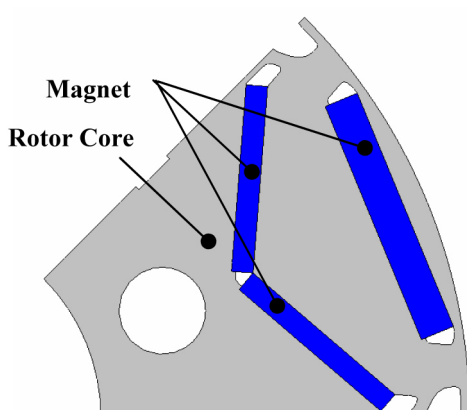
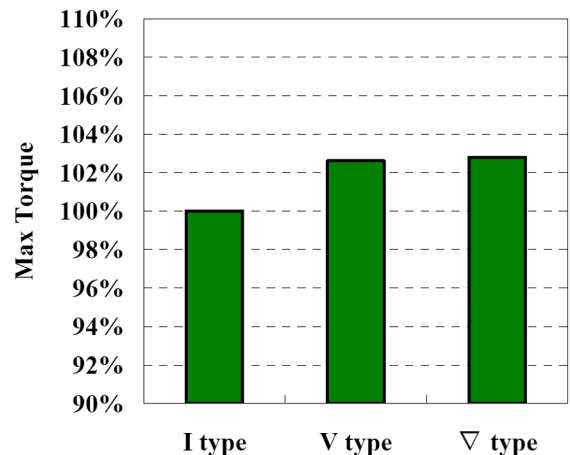
Figure 10. ∇ -Shaped rotor geometry

Figure 11. Comparison of maximum torque

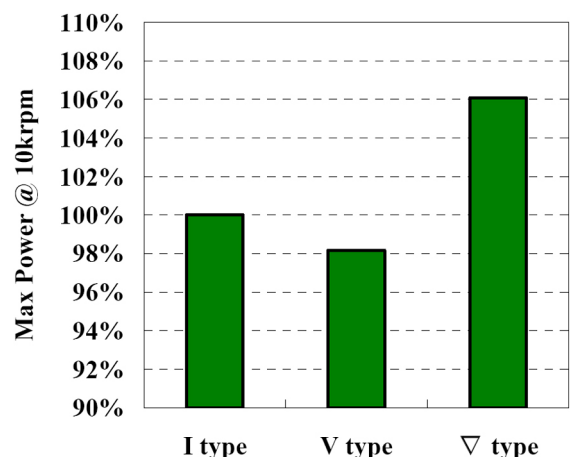


Figure 12. Comparison of maximum power in high-speed range

Compared with the I-shaped magnet arrangement that is most commonly used in embedded magnet motors, the V-shaped arrangement allows a larger magnet surface area facing an air gap. Consequently, the interlinkage magnetic flux ϕ_a becomes larger, as does the q-axis inductance because of the larger area of the electromagnetic steel sheet on the outer rim of the magnets. This results in larger reluctance torque and provides a superior torque characteristic in low-speed motor operation. However, maximum power declines in the high-speed range where field-weakening control is applied. The d-axis inductance increases owing to the large area of the electromagnetic steel sheet around the outer rim of the magnets. The magnitude of that increase is larger than the increase in the interlinkage magnetic flux ϕ_a , thereby reducing the ϕ_a/L_d ratio and causing maximum power in the high-speed region to decrease.

The ∇ -shaped rotor displays the same excellent maximum torque characteristic as the V-shaped rotor for the same reason. Moreover, it also substantially improves maximum

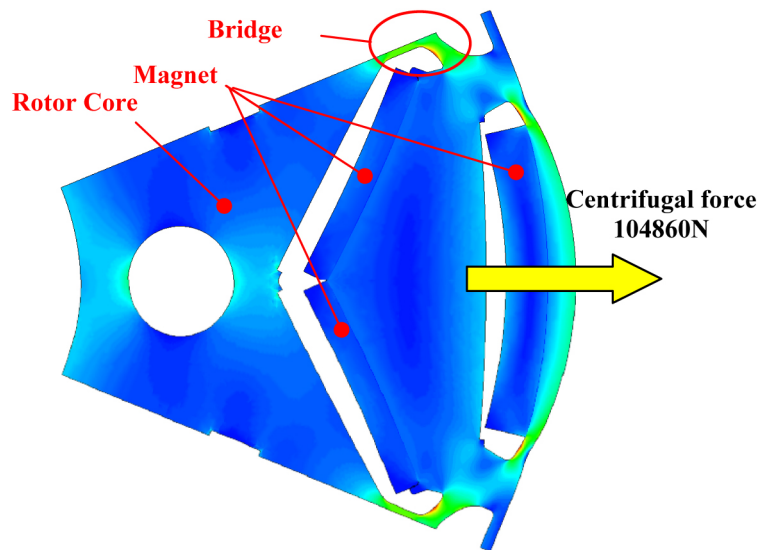


Figure 13. Simulation results for centrifugal force

power over the other two types of magnet arrangements in high-speed operation in the region of field-weakening control. In the case of this rotor, the magnets on the outer rim are smaller, allowing them to be positioned closer to the rotor surface than in the I-shaped magnet arrangement. As a result, the area of the electromagnetic steel sheet on the outer rim is smaller and the d-axis inductance is reduced, thus providing a larger ϕ_a/L_d ratio for greater maximum power.

These results indicate that the V-shaped rotor is optimally suited to an EV motor that requires both maximum torque and maximum power characteristics. This magnet arrangement was thus adopted for the drive motor of the new EV to achieve both a compact motor design and high power output.

FLUX BARRIER GEOMETRY

Flux barriers efficiently interlink the magnetic flux, produced by the magnets embedded in the rotor, from the rotor outer rim to the stator. In addition, they also function to ease the stress produced in the electromagnetic steel sheet by centrifugal force during the high-speed operation required of an EV motor.

Figure 13 shows the simulation results for the centrifugal force in the motor of the new EV when the motor is operating at its top speed. The bridges of the V-shaped magnets are needed to support the electromagnetic steel sheet and the magnets on the outside of the V-shaped magnets. The magnitude of the stress when the motor is operating at its top speed of 10390 rpm exceeds 100 kN, thus constituting a large load.

One conceivable way of reducing that stress is to increase the bridge width. However, that would increase the magnetic flux that passes through the bridges and is shunted in the rotor, thereby lowering the utilization efficiency of the magnets and causing torque to decline. To find a viable

solution, a centrifugal force simulation was conducted in which the flux barrier angle was varied as shown in Fig. 14 while keeping the bridge width constant.

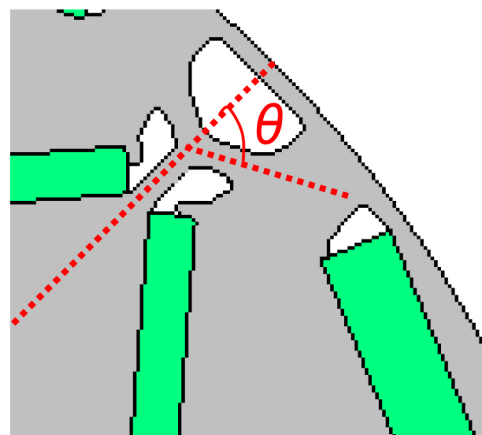


Figure 14. Bridge angle

Figure 15 shows the maximum stress level as a function of the flux barrier angle. The results indicate that stress is minimized near a barrier angle of approximately 60°. This is because the stress generated in the bridges at both ends becomes nearly equal, thereby averaging the load. These results showed that the flux barrier should be designed so that the bridges form approximately a Y-shaped geometry.

Based on these results, the flux barrier angle in the new EV motor was set at approximately 60° so as to minimize the stress level, and the bridge width was made as small as possible. These design measures improve magnet utilization efficiency by minimizing magnetic flux leakage in the rotor and contribute to the attainment of a high-efficiency motor.

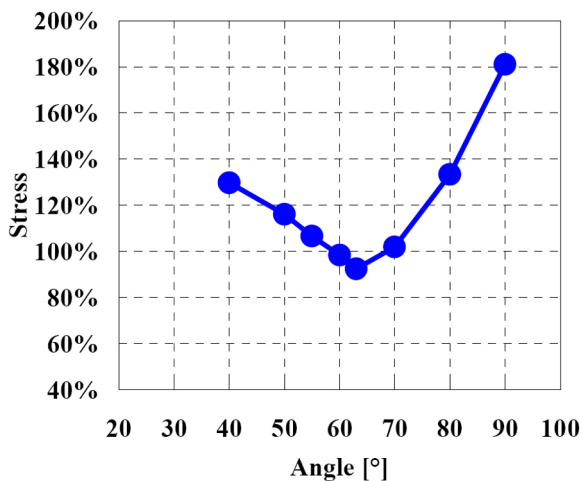


Figure 15. Stress as a function of the bridge angle

The flux barrier between the poles on the outer rim of the Y-shaped bridge substantially affects the iron loss of the motor. The eddy current and hysteresis losses W_e , W_h in the laminated core can be calculated from the harmonic flux densities [3] [4] as:

$$W_e = \sum_n \left\{ \int_{iron} K_e D(nf)^2 (B_{r,n}^2 + B_{\theta,n}^2) dv \right\} \quad (2)$$

$$W_h = \sum_n \left\{ \int_{iron} K_h D(nf) (B_{r,n}^2 + B_{\theta,n}^2) dv \right\} \quad (3)$$

where K_e and K_h are the experimental constants obtained by Epstein frame test of the core material, D is the density of the electrical steel sheets, f is the fundamental frequency, n is the order of time harmonics, $B_{r,n}$ and $B_{\theta,n}$ are the radial and peripheral components of the n -th time-harmonic flux density at each finite element.

An iron loss simulation was conducted in which the flux barrier width W_{out} was varied. Figure 16 shows the iron loss simulation results obtained for various W_{out} values. The results indicate that increasing the flux barrier width W_{out} between the poles reduces iron loss. Figure 17 shows the maximum torque at that time as a function of W_{out} . It is seen that peak torque is obtained in a certain range of W_{out} , but increasing W_{out} too much causes torque to decline.

Figure 18 shows contour diagrams of iron loss for two W_{out} values. With a larger W_{out} value, it is seen that the iron loss which occurred near the flux barrier in the q-axis magnetic path is eliminated as the core disappears, thus reducing the level of iron loss. However, the q-axis magnetic path is important for the generation of reluctance torque. Expanding the flux barrier width too much would narrow the q-axis magnetic path and reduce q-axis inductance, thereby causing the maximum torque level to decline.

Therefore, the flux barriers of the new EV motor were designed with the optimum width so as to strike a good balance between maximum torque and iron loss and thus achieve a high-efficiency motor.

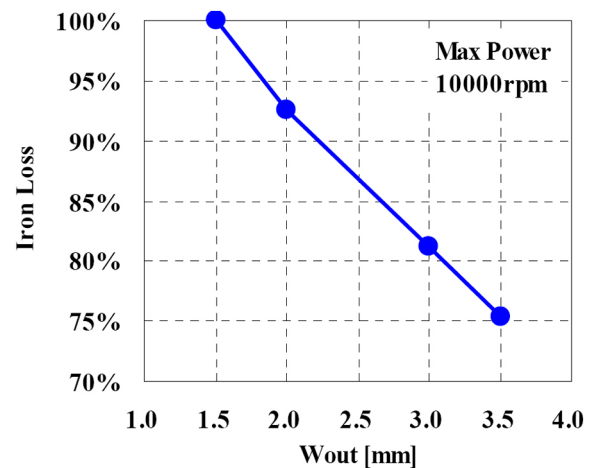


Figure 16. Iron loss as a function of W_{out}

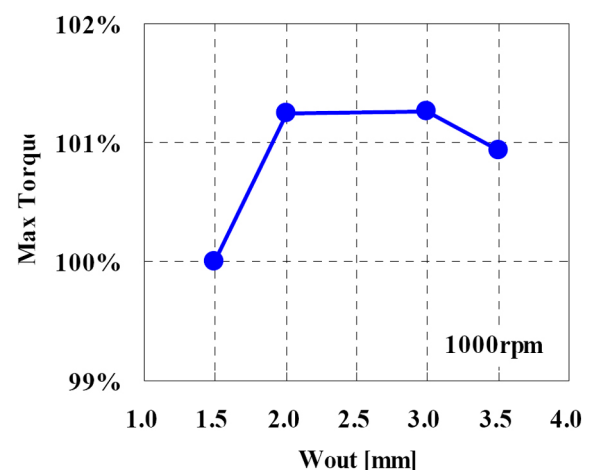


Figure 17. Maximum torque as a function of W_{out}

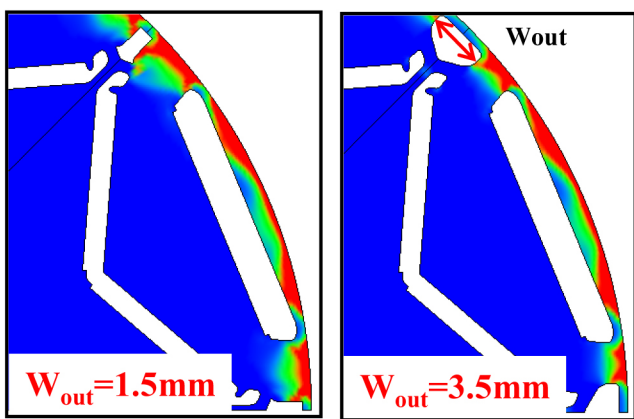


Figure 18. Iron loss simulation results

SEGMENTED MAGNETS

The Nd magnets used in EV motors suffer demagnetization as the temperature rises and that characteristic becomes the rate-limiting factor of continuous motor performance. Moreover, a large amount of dysprosium (Dy), which is a rare resource worldwide, must be added to improve the thermal resistance of Nd magnets. Accordingly, there is also a need to control the magnet temperature rise from the perspective of effective use of natural resources.

Magnet temperature rise is greatly affected by the eddy current loss that occurs in magnets themselves, in addition to the iron loss that occurs in the electromagnetic steel sheet as described earlier. One effective way of suppressing the temperature rise is to control the eddy current loss by segmenting the magnets in a layered manner similar to laminated steel as shown in Fig. 19.

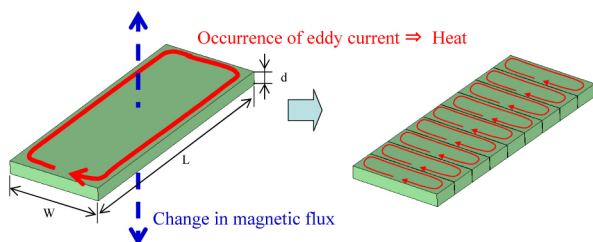


Figure 19. Eddy current control by using segmented magnets

In the case of an ideally uniform magnetic field, it is known that the eddy current loss of magnets is reduced as the number of magnet segments is increased, as shown in Eq. (4).

$$P_n = nK \frac{\pi^2 B^2 f^2}{8\rho} \frac{(L/n)^3 W^3 d}{(L/n)^2 + W^2} \quad (4)$$

where P_n is the eddy current loss, n is the number of magnet segments, W , d and L are the magnet width, thickness and length, respectively, B is the peak change in magnetic flux

density, f is the frequency, ρ is the specific resistance and K is a coefficient specific to the material.[5]

In an actual motor, the magnetic field is not uniform and magnetic flux varies in a complex manner due to the influence of slot harmonics, the harmonic components of magnetic flux, current distortion and other factors. [6][7] A motor simulation model was created using detailed mesh segmentation that took into account the eddy current in the magnets by applying electric conductivity to them. This model was used to conduct a 3-D magnetic field simulation to predict the transient eddy current response under the application of the level of current typical of high-speed motor operation.

Figure 20 shows typical results of the eddy current simulation. The results indicate that, in the case of the V-shaped magnets, the resultant eddy current flows around the entire magnet and the magnetic field of the whole magnet changes uniformly. In contrast, a local eddy current occurs in the magnets on the outer rim at places corresponding to the slots. This indicates that the eddy current is generated in the magnets due to the change in the magnetic field caused by the slot harmonics.

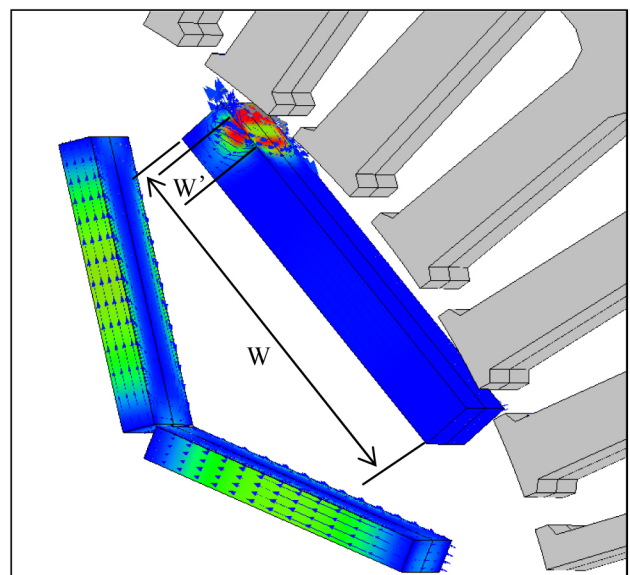


Figure 20. Eddy current simulation results

Figures 21 and 22 show the results obtained with the theoretical expression in Eq. (4) and the magnetic field simulation using the motor model to predict the eddy current in the magnets, when the number of magnet segments was varied. The results for the V-shaped magnets in Fig. 21 show that the magnetic loss reduction effect obtained by increasing the number of magnet segments nearly coincided with the theoretical value. This suggests that the eddy current loss in the magnets was produced by the uniform change in the magnetic field. In contrast, the results for the outer rim magnets in Fig. 22 show that the loss reduction effect was smaller than the theoretical value. This presumably indicates that the eddy current generated by the slot harmonics

occurred in only some of the magnets. The value of the magnet width W in Eq. (4) was not the original magnet width, but rather the width W' of an equivalent local eddy current, which would account for the results seen in the figure 20.

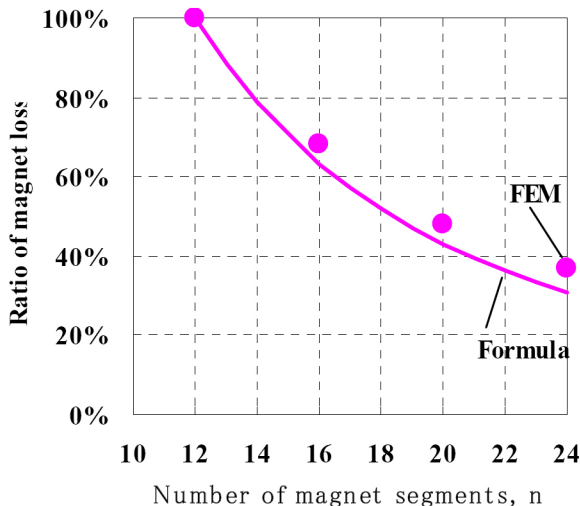


Figure 21. Effect of number of magnet segments on reducing eddy current loss (V-shaped magnets)

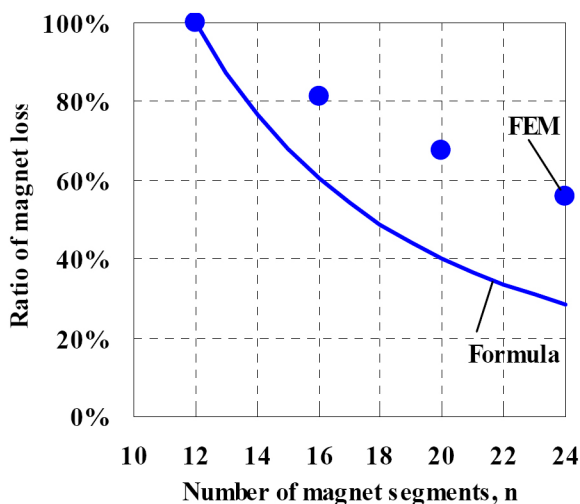


Figure 22. Effect of number of magnet segments on reducing eddy current loss (outer rim magnets)

In the motor developed for the new EV, the magnets are divided into 18 segments, taking into account the upper temperature limit of the magnets and the temperature rise due to the losses that occur. This design measure achieves high continuous motor performance and high efficiency, while eliminating the use of Dy.

SUMMARY/CONCLUSIONS

This paper has described a newly developed permanent magnet synchronous motor for EV application that generates maximum torque of 280 Nm and maximum power of 80 kW.

This new motor was selected as the first electrified powertrain to be included in Ward's 10 Best Engines list for 2011.

In the process of developing this motor, the results of magnet field simulations and mechanical strength simulations were used to achieve a compact motor size, high output and high efficiency through the application of the following in-house technologies.

- A rotor geometry with interior permanent magnets arranged in the ∇ -shape for an outstanding balance of motor torque and power.
- V-shaped magnetic flux barriers that provide both exceptional mechanical strength and performance during high-speed motor operation.
- Specially designed flux barrier geometry on the outer rim to reduce iron loss.
- Segmented magnets that facilitate high continuous motor performance and high efficiency while also conserving rare metal resources.

REFERENCES

1. Sato, Y., Ishikawa, S., Okubo, T., Abe, M. et al., "Development of High Response Motor and Inverter System for the Nissan LEAF Electric Vehicle," SAE Technical Paper [2011-01-0350](#), 2011, doi: [10.4271/2011-01-0350](#).
2. Honda, Y., Nakamura, T., Higaki, T., Takeda, Y., "Motor Design Considerations and Test Results of an Interior Permanent Magnet Synchronous Motor for Electric Vehicles," Industry Applications Conference, 1997. Thirty-Second IAS Annual Meeting, IAS '97, Conference Record of the 1997 IEEE doi: [10.1109/IAS.1997.643011](#) Page(s): 75-82 vol. 1.
3. Yamazaki, K. and Seto, Y., "Iron Loss Analysis of Interior Permanent Magnet Synchronous Motors-Variation of Main Loss Factors Due to Driving Condition", IEEE Trans. on Ind. Appl., vol. 42, no. 4, pp. 1045-1052, 2006.
4. Yamazaki, K., Oki, S., Nezu, A., Ikemi, T., "Development of Interior Permanent Magnet Motors Reduction of Harmonic Iron Losses by Optimizing Rotor Structures," Electric Machines & Drives Conference, 2007. IEMDC '07. IEEE International, p489-494, doi: [10.1109/IEMDC.2007.382716](#).
5. Aoyama, Y., Ohashi, K. and Miyata, K., "Experiment and Analysis of Eddy Current Loss in Permanent Magnet under Alternating Magnetic Field," Paper of the Rotating Machinery Workshop, IEE of Japan, RM-02-135, (2002) (in Japanese).
6. Yamazaki, K., Abe, A., "Loss Investigation of Interior Permanent-Magnet Motors Considering Carrier Harmonics and Magnet Eddy Currents," Industry Applications, IEEE Transactions on, Volume: 45, Issue: 2, 2009, Page(s): 659-665
7. Yamazaki, K., Kanou, Y., Fukushima, Y., Oki, S., Nezu, A., Ikemi, T. and Mizokami, R., "Reduction of Magnet Eddy Current Loss in Interior Permanent Magnet Motors with Concentrated Windings," Industry Applications, IEEE Transactions on, Volume: 46, Issue: 6, 2010, Page(s): 2434-2441

CONTACT INFORMATION

NISSAN MOTOR CO., LTD.
10-1, Hironodai 2-chome, Zama-shi
Kanagawa 228-8502, Japan
Phone: +81-50-2029-4373
s-ohki@mail.nissan.co.jp